Chapter 14 Analytical Trial Function Method Ⅰ— Membrane and Plate Bending Elements

Song Cen
Department of Engineering Mechanics, School of Aerospace,
Tsinghua University, Beijing, 100084, China

Zhi-Fei Long
School of Mechanics & Civil Engineering, China University of
Mining & Technology, Beijing, 100083, China

Abstract This chapter introduces a novel finite element method, namely, the analytical trial function method. A detailed discussion on the features of the analytical trial function method is firstly given in Sect. 14.1. Then, in the next five sections, the basic analytical solutions of plane problem, thick plate problem and thin plate problem are derived and taken as the trial functions for the corresponding finite element models. It can be seen that those resulting models exhibit excellent performance. Some challenging problems, such as the trapezoidal locking and shear locking, can be avoided naturally.

Keywords finite element, analytical trial function method, membrane element, plate bending element.

14.1 Recognition of the Analytical Trial Function Method

14.1.1 Trial Function

When constructing a displacement-based element, the first step is usually to assume its displacement mode. For example, the displacement mode of the constant strain triangular element CST is assumed to be

$$\begin{Bmatrix} u \\ v \end{Bmatrix} = \begin{bmatrix} 1 & 0 & x & 0 & y & 0 \\ 0 & 1 & 0 & x & 0 & y \end{bmatrix} \begin{Bmatrix} \lambda_1 \\ \vdots \\ \lambda_6 \end{Bmatrix} = \boldsymbol{F}\boldsymbol{\lambda} \tag{14-1}$$

and the displacement mode of the rectangular thin plate element ACM is assumed to be

$$w=[1 \quad x \quad y \quad x^2 \quad xy \quad y^2 \quad x^3 \quad x^2y \quad xy^2 \quad y^3 \quad x^3y \quad xy^3]\begin{Bmatrix}\lambda_1\\ \vdots \\ \lambda_{12}\end{Bmatrix}=\boldsymbol{F}\boldsymbol{\lambda} \tag{14-2}$$

where $\boldsymbol{\lambda}$ is the undetermined parameter vector; $\boldsymbol{F}$ is composed of trial functions (or basis functions).

Element performance relies deeply on the selected trial functions. As a result of the irrationally selected trial functions for displacements, trapezoidal locking and shear locking phenomena may exist in some membrane and thick plate elements, respectively.

14.1.2 Analytical Trial Function

In structural matrix analysis, the exact (or analytical) solutions for the displacement of the thin beam theory are used by the thin beam element. That is to say, the selected trial functions are analytical solutions; therefore, they are called as *analytical trial functions*.

Timoshenko thick beam element also uses the exact solutions for the displacements of the thick beam theory. So, it will not suffer from shear locking phenomenon because the analytical trial functions are employed.

2D and 3D elasticity problems, thin and thick plate problems are all problems with infinite DOFs. For their homogeneous problems, the analytical solutions are composed of infinite terms. Finite element method is an approximate method in which such infinite DOF problems are treated as problems with only finite DOFs. And, the corresponding element model also contains finite (n) DOFs, which means that its displacement mode contains only n basic analytical trial functions. These n analytical solutions can be selected in turn from low to high orders.

14.1.3 Analytical Trial Function Method

The construction procedure of the finite element model in which the basic analytical solutions are taken as the trial functions is called *the finite element method based on analytical trial functions*, or *the analytical trial function method*.

The feature of the analytical trial function method is: the finite element method is a discrete approximate method, while the advantages of the analytical method are preserved in it. It exhibits the close relation between the trial function and the

basic analytical solution and the complementarity between discrete and analytical methods.

14.1.4 Recognition of the Analytical Trial Function Method

At the beginning of the finite element method, all people thought of taking the most basic analytical solutions as the trial functions. For instance, in the displacement mode (14-1) of the first membrane element CST, the selected 6 trial functions are just the most basic analytical solutions of the 2D homogenous problem in elasticity (3 rigid body displacements and 3 constant strain states). And, in the displacement mode (14-2) of the first rectangular thin plate element ACM, the selected 12 trial functions are just the most basic analytical solutions of the thin plate homogenous problem, i.e., they are all the analytical solutions of the following homogenous differential equation

$$\nabla^2\nabla^2 w = 0 \tag{14-3}$$

and are the 12 analytical solutions of the lowest orders which contain 3 rigid body displacement states, 3 constant strain states, 4 linear strain states and 2 quadratic strain states. It can be seen that, for these earliest elements, whether by conscious efforts or not, their construction procedures are in keeping with the requirement of the analytical trial function method. That is to say, the analytical trial function method is the earliest scheme used in the finite element method.

With the flourishing development of the finite element method, various schemes have been proposed one after the other. Especially, after the isoparametric elements were broadly used, the analytical trial function method was almost overlooked.

Owing to the inherent advantages of the analytical trial function method, its new applications are continuously suggested in some references. For example, in 1982, reference [1] used the analytical solutions containing singular stress point as the trial functions for developing the singular element with crack, which provides an effective solution scheme for the crack problem; in 1996, reference [2] proposed a rational finite element method, and constructed a set of high quality elements by using the basic analytical solutions for plane elasticity; reference [3] takes the basic analytical solutions of the thick plate theory as the trial functions to develop the thick plate elements, which rationally resolves the matching problem of the trial functions for deflection and rotations so that shear locking phenomenon can be eliminated from the outset; reference [4] uses the analytical solutions to construct two membrane elements which can keep high precision in distorted mesh, and the trapezoidal locking problem given in reference [5] is thus solved. In 2002, reference [6] gave a systematical review of the analytical trial function method. It points out the advantages and potentialities of the analytical trial function method in dealing with mesh distortion, shear locking and singular

stress point problems, which will induce further studies and developments on the analytical trial function method.

14.2 4-Node Membrane Elements Based on the Analytical Trial Function Method

14.2.1 The Basic Analytical Solutions in Plane Elasticity

In plane elasticity, the analytical solutions of different order which satisfy the basic governing equations, including equilibrium equations, geometrical equations and constitutive law, can be derived. The 12 low-order analytical solutions are listed in Table 14.1 (in which μ is the Poisson's ratio).

Table 14.1 The basic analytical solutions in plane elasticity

No.of terms	1	2	3	4	5	6	7	8	9	10	11	12
u	1	0	y	y	$-\mu x$	x	$-\mu x^2-y^2$	$2xy$	$-2\mu xy$	$x^2-(2+\mu)y^2$	$-3\mu x^2y-y^3$	$3yx^2-(2+\mu)y^3$
v	0	1	$-x$	x	y	$-\mu y$	$2xy$	$-\mu y^2-x^2$	$y^2-(2+\mu)x^2$	$-2\mu xy$	$3xy^2-(2+\mu)x^3$	$-3\mu y^2x-x^3$
θ	0	0	1	0	0	0	$-2y$	$2x$	$2x$	$-2y$	$3x^2-3y^2$	$3x^2-3y^2$
ε_x	0	0	0	0	$-\mu$	1	$-2\mu x$	$2y$	$-2\mu y$	$2x$	$-6\mu xy$	$6xy$
ε_y	0	0	0	0	1	$-\mu$	$2x$	$-2\mu y$	$2y$	$-2\mu x$	$6xy$	$-6\mu xy$
γ_{xy}	0	0	0	2	0	0	0	0	$-4(1+\mu)x$	$-4(1+\mu)y$	$-6(1+\mu)x^2$	$-6(1+\mu)y^2$

14.2.2 3 Membrane Elements Based on the Analytical Trial Functions

A 4-node, 8-DOF membrane element shown in Fig. 14.1 is considered. The element nodal displacement vector is

$$\boldsymbol{q}^e = [u_1 \quad v_1 \quad u_2 \quad v_2 \quad u_3 \quad v_3 \quad u_4 \quad v_4]^{\mathrm{T}} \tag{14-4}$$

By using the first eight terms of the analytical solutions given in Table 14.1 as the trial functions, the element displacements u and v are assumed to be

$$\begin{Bmatrix} u \\ v \end{Bmatrix} = \begin{bmatrix} 1 & 0 & y & y & -\mu x & x & -\mu x^2-y^2 & 2xy \\ 0 & 1 & -x & x & y & -\mu y & 2xy & -\mu y^2-x^2 \end{bmatrix} \begin{Bmatrix} \lambda_1 \\ \lambda_2 \\ \vdots \\ \lambda_8 \end{Bmatrix} \tag{14-5}$$

where $\lambda_1, \lambda_2, \cdots, \lambda_8$ are 8 unknown parameters.

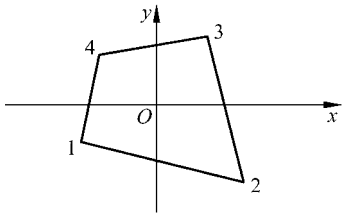

Figure 14.1 A 4-node quadrilateral membrane element

By employing 8 nodal conforming conditions

$$\left.\begin{aligned}(u-\overline{u})_i &= 0\\ (v-\overline{v})_i &= 0\end{aligned}\right\} \quad (i=1,2,3,4) \tag{14-6}$$

the 8 unknown parameters can be solved and expressed in terms of $\boldsymbol{q}^e$. This element is denoted as ATF-Q4a.

If the 8 nodal conforming conditions are replaced by the following nodal and perimeter conforming conditions

$$\left.\begin{aligned}
&\iint_{A^e}\frac{\partial u}{\partial x}\mathrm{d}A=\oint_{\partial A^e} l\overline{u}\mathrm{d}s && \iint_{A^e}\frac{\partial v}{\partial x}\mathrm{d}A=\oint l\overline{v}\mathrm{d}s\\
&\iint_{A^e}\frac{\partial u}{\partial y}\mathrm{d}A=\oint m\overline{u}\mathrm{d}s && \iint_{A^e}\frac{\partial v}{\partial y}\mathrm{d}A=\oint m\overline{v}\mathrm{d}s\\
&\sum_{i=1}^{4}(u-\overline{u})_i=0 && \sum_{i=1}^{4}(v-\overline{v})_i=0\\
&\sum_{i=1}^{4}(u-\overline{u})_i\xi_i\eta_i=0 && \sum_{i=1}^{4}(v-\overline{v})_i\xi_i\eta_i=0
\end{aligned}\right\} \tag{14-7}$$

in which l and m are the direction cosines of the normal on the element boundary; ξ_i and η_i are the isoparametric coordinates of node i; $\overline{u}$ and $\overline{v}$ are the displacements of the element boundary. This element is denoted as ATF-Q4b.

For the 4-node membrane element shown in Fig. 14.1, if the rotation θ_i of node i is also taken as the DOF, the element will have 12 DOFs. Thus, the element nodal displacement vector is

$$\boldsymbol{q}^e=[u_1 \quad v_1 \quad \theta_1 \quad u_2 \quad v_2 \quad \theta_2 \quad u_3 \quad v_3 \quad \theta_3 \quad u_4 \quad v_4 \quad \theta_4]^{\mathrm{T}} \tag{14-8}$$

The 12 analytical solutions given in Table 14.1 are taken as the trial functions, and the following 12 nodal conforming conditions

$$\left.\begin{aligned}(u-\overline{u})_i &= 0\\ (v-\overline{v})_i &= 0\\ (\theta-\overline{\theta})_i &= 0\end{aligned}\right\} \quad (i=1,2,3,4) \tag{14-9}$$

are also used, in which

$$\theta=\frac{1}{2}\left(\frac{\partial u}{\partial y}-\frac{\partial v}{\partial x}\right) \tag{14-10}$$

This element is denoted as ATF-Q4θ.

14.3 Avoiding Trapezoidal Locking Phenomenon by ATF Elements

As to the trapezoidal locking problem (or sensitivity problem to mesh distortion), the analytical trial function method provides an effective solution countermeasure.

Example 14.1 Sensitivity test Ⅰ to mesh distortion—A pure bending beam divided by two distorted elements.

A cantilever beam subjected to pure bending load is shown in Fig. 14.2, and it is divided into two elements. δ is a distortion parameter. When δ increases, the distortion will become more serious. The length of the beam is 10; height is 2; thickness is 1. And, $E=1500$, $\mu=0.25$. Results of the deflection v_A at tip A are plotted in Fig. 14.3. Besides the present elements ATF-Q4a, ATF-Q4b and ATF-Q4θ, results obtained by the 4-node isoparametric element Q4, the isoparametric element with internal parameters QM6[7] and the hybrid stress element P-S[8] are also given for comparison.

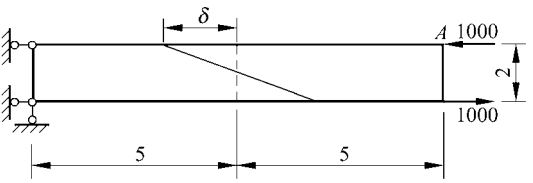

Figure 14.2 A beam divided by two distorted elements

From Fig. 14.3, it can be seen that, the precision of the 4-node isoparametric element Q4 is the lowest: when $\delta=0$, since the length-height ratio of the rectangular element is high $\left(\frac{L}{h}=\frac{5}{2}\right)$, the precision of v_A has already dropped to 28%. And, with the increase of δ, its precision will continually drop, even below

10%. Though the precisions of the hybrid stress element P-S, the isoparametric element with internal parameters QM6 and element ATF-Q4b are all 100% for the rectangular element case (δ= 0), if δ>1, they will be below 60%. The precisions of the other two present elements ATF-Q4a and ATF-Q4θ are the best: with the increase of the distortion parameter δ, the precision can always keep 100% which means that both the elements are very insensitive to mesh distortion. From these results, it can be concluded that, if appropriate conforming conditions are selected, ATF elements can exhibit excellent performance for avoiding trapezoidal locking.

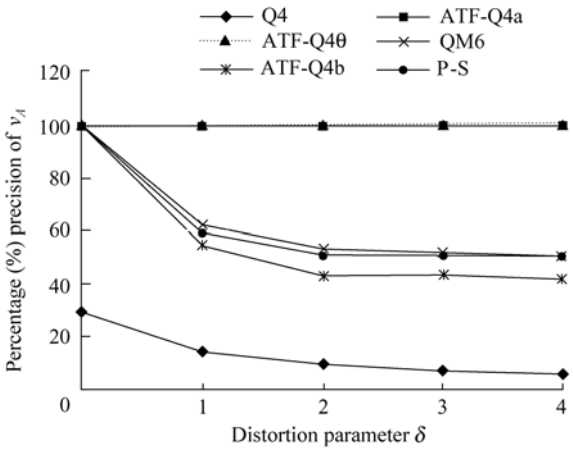

Figure 14.3 Relation between Percentage (%) precision of v_A and distortion parameter δ

Example 14.2 Sensitivity test Ⅱ to mesh distortion—MacNeal thin beam problem with distorted mesh.

The MacNeal thin beam problem[5] is shown in Fig. 14.4, in which rectangular, parallelogram and trapezoidal mesh are used. This is a famous benchmark for testing the sensitivity to mesh distortion. The precisions of many 4-node membrane

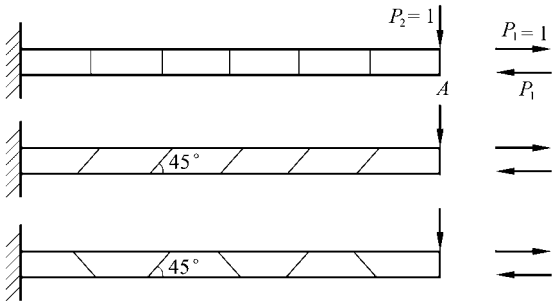

Figure 14.4 MacNeal thin beam with distorted meshes

elements drop dramatically for the trapezoidal mesh case, which is the so-called trapezoidal locking phenomenon. The length of the cantilever beam is 6, the height is 0.2; the elastic constants $E = 10^7$ and $\mu = 0.3$. Two tip load cases are considered: pure bending and transverse shear.

The results of the deflection v_A at tip A are listed in Table 14.2. Besides the present three elements, the results obtained by the 4-node isoparametric element Q4, hybrid stress element P-S[8], 4-node element QUAD4[5] with one integration point, assumed strain element PEAS7[9] and its modification versions, the elements M1PEAS7 and M2PEAS7[10] are also given for comparison.

Table 14.2 The percentage (%) precision of the tip deflection v_A of MacNeal beam

Load case	Transverse shear			Pure bending		
Mesh	Rectangle	Parallelogram	Trapezoid	Rectangle	Parallelogram	Trapezoid
Q4	9.3	3.5	0.3	9.3	3.1	2.2
QUAD4	90.4	8.0	7.1			
P-S	99.3	79.8	22.1	100	85.2	16.7
PEAS7	98.2	79.5	21.7			
M1PEAS7	99.3	94.8	36.7			
M2PEAS7	99.3	94.3	36.8			
ATF-Q4b	99.4	61.3	4.5	100	70.7	4.1
ATF-Q4a	99.4	99.4	99.4	100	100	100
ATF-Q4θ	100	100	100	100	100	100

From Table 14.2, it can be seen that, because the length-height ratio of the element is $1/0.2 = 5$, the precision of the element Q4 drops obviously. The element QUAD 4 using a single integration point is seriously locking in parallelogram and trapezoidal meshes. The precisions of the hybrid stress element P-S, element ATF-Q4b, assumed strain elements PEAS7, M1PEAS7 and M2PEAS7 are similar: for the mesh divided by rectangular elements, the precision is the best; for the mesh divided by parallelogram elements, the precision will drop; and for the mesh divided by trapezoidal elements, locking phenomenon will happen. Only two elements ATF-Q4a and ATF-Q4θ, which are proposed in this section, possess high accuracy for all mesh divisions, i.e., they are insensitive to mesh distortion. And, element ATF-Q4θ can even provide exact solutions for the two load cases and three meshes. The trapezoidal locking problem of MacNeal beam is a serious challenge to the 4-node, 8-DOF membrane elements. The victory of the element ATF-Q4a in this challenge exhibits its advantage again.

Example 14.3 Weak patch test for the element ATF-Q4a.

Patch test is often used for testing the convergence of the non-conforming elements. It has two forms:

Strict form—The boundary conditions are specified according to the constant strain state. Then, by using an arbitrary mesh divided by the elements with finite

dimensions, the finite element solutions will be tested to see whether they are the exact solutions.

Weak form—The boundary conditions are also specified according to the constant strain state. Then, by using meshes refined by more and more elements, the finite element solutions will be tested to see whether they are convergent to the exact ones.

The merit of the strict form is that it can be conveniently performed; and the merit of the weak form is that it possesses the right description and is more coincident with the original idea of the convergence.

The MacNeal beam subjected to a horizontal load (resultant force is 1) is considered. This structure is under a constant strain state. By using the two refined meshes shown in Fig. 14.5, the convergence of the element ATF-Q4a is analyzed. The results of the tip displacement are listed in Table 14.3 (the analytical solution is 0.6).

In Fig. 14.5, the refined mesh A firstly contains $n\times n$ rectangular elements; then, each rectangular element is divided into two trapezoidal elements, thus, $2n^2$ elements are totally obtained. And, the refined mesh B firstly contains two trapezoidal elements; then, each trapezoidal element is bisected through the midpoints of the element sides so that it is divided into four trapezoidal elements; finally, $2n^2$ elements are totally obtained.

From Table 14.3, it can be seen that the element ATF-Q4a cannot pass the strict patch test because it does not produce the exact solutions of the constant strain state by mesh with finite dimensions. But, with the refinement of the mesh, the finite element solutions can rapidly converge to the exact solutions. So, the element ATF-Q4a can pass the weak patch test.

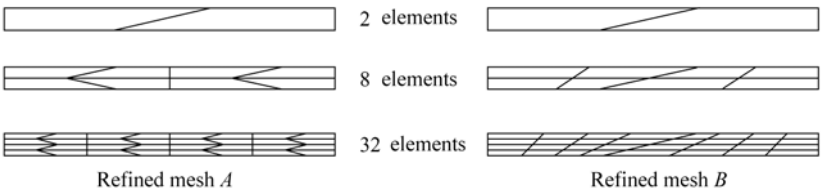

Figure 14.5 Two refined patterns of the meshes for MacNeal beam

Let us make a comparison between the elements ATF-Q4a and ATF-Q4b. From the numerical results of Examples 14.1 and 14.2, it can be seen that the precision of the element ATF-Q4a is obviously higher than that of the element ATF-Q4b. But, the element ATF-Q4b can pass the strict patch test (thereby it can also pass the weak one), and the element ATF-Q4a can only pass the weak patch test. By this token, the ultimate rule for testing the convergence should be the weak patch test, not the strict one. It is not appropriate to deny the element ATF-Q4a, which possesses high accuracy, only according to the results of the strict patch test.

Table 14.3 The tip displacements of the MacNeal beam under tension (ATF-Q4a)

Num. of elements	Refined mesh *A*		Refined mesh *B*	
	Result	Relative Precision	Result	Relative Precision
2	0.6923	1.1538	0.6923	1.1538
	0.6923	1.1538	0.6923	1.1538
8	0.5935	0.9892	0.6067	1.0112
	0.6318	1.0530	0.5998	0.9997
	0.5935	0.9892	0.6065	1.0108
32	0.6008	1.0013	0.6014	1.0023
	0.6010	1.0017	0.6003	1.0005
	0.6010	1.0017	0.5997	0.9995
	0.6010	1.0017	0.5988	0.9980
	0.6008	1.0013	0.6029	1.0048

14.4 The Basic Analytical Solutions of the Thick Plate Theory and ATF Elements Free of Shear Locking

14.4.1 Shear Locking Phenomenon in the Thick Plate Element

During the construction procedure of the thick plate element based on the Mindlin-Reissner thick plate theory, the three displacement components w, ψ_x and ψ_y should be independent variables. When the thick plate degenerates to be a thin plate, then, according to the Kirchhoff thin plate theory, the rotations ψ_x and ψ_y will be the derivatives of w, which are not independent anymore. Many displacement-based elements produce false shear strains γ_x and γ_y in thin plate cases, consequently, shear locking phenomenon will happen. Reference [11] claimed that, "The root of this difficulty lies on the contradiction of the double requirements of dependence and independence among the displacements". In order to overcome such shear locking, many countermeasures have already been proposed in numerous literatures. The most popular countermeasures are reduced integration[12] and selected reduced integration schemes[13]. However, though they can provide us temporary solutions, the shear locking is still not eliminated from the outset, and even some new troubles, such as spurious zero energy mode, may be aroused. In some recent references [14 – 18], the double requirements of dependence and independence among the displacements have been translated into other double requirements of nonzero and zero shear strains, and a rational interpolation scheme for shear strains which satisfies the double requirements is proposed. As a result, a series of thick plate elements which can completely

avoid shear locking are developed successfully. This section will present another way to eliminate shear locking: The basic analytical solutions of the Mindlin-Reissner theory are used in the trial functions of the thick plate displacements w, ψ_x and ψ_y; when the plate degenerates to be a thin plate, these basic analytical solutions will automatically degenerate to be those of the Kirchhoff theory, and consequently, the shear locking will also be avoided from the outset.

14.4.2 The Basic Analytical Solutions of the Thick Plate Theory

In the equilibrium differential equations of the thick plate, if the internal forces are expressed in terms of the displacements, the basic differential equations of the displacement method for the thick plate can be obtained. For the homogeneous problem when all loads are zero, we have

$$\left.\begin{aligned} &D\left(\frac{\partial^2\psi_x}{\partial x^2}+\frac{1-\mu}{2}\frac{\partial^2\psi_x}{\partial y^2}+\frac{1+\mu}{2}\frac{\partial^2\psi_y}{\partial x\partial y}\right)+C\left(\frac{\partial w}{\partial x}-\psi_x\right)=0\\ &D\left(\frac{1+\mu}{2}\frac{\partial^2\psi_x}{\partial x\partial y}+\frac{1-\mu}{2}\frac{\partial^2\psi_y}{\partial x^2}+\frac{\partial^2\psi_y}{\partial y^2}\right)+C\left(\frac{\partial w}{\partial y}-\psi_y\right)=0\\ &C\left(\frac{\partial^2 w}{\partial x^2}+\frac{\partial^2 w}{\partial y^2}-\frac{\partial\psi_x}{\partial x}-\frac{\partial\psi_y}{\partial y}\right)=0 \end{aligned}\right\} \tag{14-11}$$

Let $F(x, y)$ be a bi-harmonic function which satisfies the following bi-harmonic equation

$$\nabla^2\nabla^2 F=0 \tag{14-12}$$

where

$$\nabla^2=\frac{\partial^2}{\partial x^2}+\frac{\partial^2}{\partial y^2}$$

Then, the following expressions

$$w=F-\frac{D}{C}\nabla^2 F,\quad \psi_x=\frac{\partial F}{\partial x},\quad \psi_y=\frac{\partial F}{\partial y} \tag{14-13}$$

are the solutions of Eq. (14-11). Let d be a characteristic length. By introducing the dimensionless coordinates ξ and η

$$\xi=\frac{x}{d},\quad \eta=\frac{y}{d} \tag{14-14}$$

and the dimensionless parameter λ

$$\lambda = \frac{D}{Cd^2} = \frac{h^2}{5(1-\mu)d^2} \tag{14-15}$$

the first expression in Eq. (14-13) can be written as

$$w = F - \lambda\left(\frac{\partial^2}{\partial\xi^2} + \frac{\partial^2}{\partial\eta^2}\right)F \tag{14-16}$$

If $\frac{h}{d} \to 0$, $\lambda \to 0$, then, the analytical solutions (14-13) of the thick plate theory will degenerate to be the following analytical solutions of the thin plate theory

$$\left.\begin{aligned} &w = F, \quad \psi_x = \frac{\partial F}{\partial x}, \quad \psi_y = \frac{\partial F}{\partial y} \\ &\gamma_{xz} = \frac{\partial w}{\partial x} - \psi_x = 0, \quad \gamma_{yz} = \frac{\partial w}{\partial y} - \psi_y = 0 \end{aligned}\right\} \tag{14-17}$$

From above, it can be concluded that, if the basic analytical solutions (14-13) of the thick plate theory are taken as the trial functions for the thick plate element, once $\frac{h}{d} \to 0$, these trial functions will automatically degenerate to be the analytical solutions of the thin plate theory, thereby, the shear locking phenomenon can be eliminated from the outset.

14.5 Development of Quadrilateral Thin-Thick Plate Element Based on the Analytical Trial Function Method

14.5.1 Thick Plate Element ATF-MQ Based on the Analytical Trial Function Method

Consider a quadrilateral thick plate element with 12 DOFs, its nodal displacement vector is

$$\boldsymbol{q}^e = [w_1 \quad \psi_{x1} \quad \psi_{y1} \quad w_2 \quad \psi_{x2} \quad \psi_{y2} \quad w_3 \quad \psi_{x3} \quad \psi_{y3} \quad w_4 \quad \psi_{x4} \quad \psi_{y4}]^{\mathrm{T}}$$

According to the analytical solutions (14-13) of the thick plate theory, the first 12 low-order terms of the analytical solutions are taken as the trial functions. The

element displacements w, ψ_x and ψ_y can be expressed by

$$\begin{Bmatrix} w \\ \psi_x \\ \psi_y \end{Bmatrix} = \begin{bmatrix} 1 & x & y & x^2-2\frac{D}{C} & xy & y^2-2\frac{D}{C} & x^3-6\frac{D}{C}x & x^2y-2\frac{D}{C}y \\ 0 & 1 & 0 & 2x & y & 0 & 3x^2 & 2xy \\ 0 & 0 & 1 & 0 & x & 2y & 0 & x^2 \end{bmatrix}$$

$$\begin{bmatrix} xy^2-2\frac{D}{C}x & y^3-6\frac{D}{C}y & x^3y-6\frac{D}{C}xy & xy^3-6\frac{D}{C}xy \\ y^2 & 0 & 3x^2y & y^3 \\ 2xy & 3y^2 & x^3 & 3xy^2 \end{bmatrix} \boldsymbol{\lambda} \tag{14-18}$$

where D is the bending stiffness of the plate; C is the shear stiffness of the plate; $\boldsymbol{\lambda}$ is a vector composed of 12 parameters.

The corresponding curvature fields $\boldsymbol{\kappa} = [\kappa_x \quad \kappa_y \quad 2\kappa_{xy}]^{\mathrm{T}}$ are

$$\begin{Bmatrix} \kappa_x \\ \kappa_y \\ 2\kappa_{xy} \end{Bmatrix} = \begin{bmatrix} 0 & 0 & 0 & -2 & 0 & 0 & -6x & -2y & 0 & 0 & -6xy & 0 \\ 0 & 0 & 0 & 0 & 0 & -2 & 0 & 0 & -2x & -6y & 0 & -6xy \\ 0 & 0 & 0 & 0 & -2 & 0 & 0 & -4x & -4y & 0 & -6x^2 & -6y^2 \end{bmatrix} \boldsymbol{\lambda} \tag{14-19}$$

And, the corresponding shear strain fields $\boldsymbol{\gamma} = [\gamma_{xz} \quad \gamma_{yz}]^{\mathrm{T}}$ are

$$\begin{Bmatrix} \gamma_{xz} \\ \gamma_{yz} \end{Bmatrix} = \begin{bmatrix} 0 & 0 & 0 & 0 & 0 & 0 & -6\frac{D}{C} & 0 & -2\frac{D}{C} & 0 & -6\frac{D}{C}y & -6\frac{D}{C}y \\ 0 & 0 & 0 & 0 & 0 & 0 & 0 & -2\frac{D}{C} & 0 & -6\frac{D}{C} & -6\frac{D}{C}x & -6\frac{D}{C}x \end{bmatrix} \boldsymbol{\lambda} \tag{14-20}$$

The following 12 nodal and line conforming conditions

$$\left.\begin{aligned} &(w-\tilde{w})_i = 0 && \text{(for each node } i = 1,2,3,4) \\ &(\psi_s - \tilde{\psi}_s)_i = 0 && \text{(for the end point } i \text{ of each side } d_{ij}\text{: } i = 1,2,3,4) \\ &\int_{d_{ij}} (\psi_n - \tilde{\psi}_n)\mathrm{d}s = 0 && \text{(for each side } ij = 12,23,34,41) \end{aligned}\right\} \tag{14-21}$$

are employed, in which n and s are the normal and tangential directions of each element side; $\tilde{w}$, $\tilde{\psi}_s$ and $\tilde{\psi}_n$ are the displacements along the element boundary. Thus, the 12 parameters in $\boldsymbol{\lambda}$ can be obtained and expressed in terms of $\boldsymbol{q}^e$. This element is denoted as ATF-MQ.

14.5.2 Numerical Examples

Example 14.4 The central deflection of the simply-supported and clamped square plates under uniformly distributed load.

Two thickness-span cases, ① thick plate ($h/L = 0.3$)and ② thin plate ($h/L = 0.003$), are considered. The central deflection w_C is computed by the element ATF-MQ using different mesh density. Its relative precision is given in Table 14.4.

Table 14.4 The relative precision for the central deflection w_C of square plate (ATF-MQ)

Mesh	Thick plate ($h/L = 0.3$)		Thin plate ($h/L = 0.003$)	
	Simply-supported	Clamped	Simply-supported	Clamped
2×2	1.009	1.035	1.011	1.009
4×4	1.002	1.006	1.003	1.006
8×8	1.0005	0.9998	1.0007	1.003
16×16	1.0002	0.9984	1.0001	1.002
32×32	1.0001	0.9980	1.0001	1.002

From Table 14.4, it can be seen that the element ATF-MQ exhibits excellent performance for both thick and thin plates, and no shear locking happens. For the simply-supported and clamped square plates, high accuracy can be obtained. When a 8×8 mesh is used, all relative errors are below 0.3%.

Example 14.5 The central deflection and bending moment of the simply-supported and clamped circular plates under uniformly distributed load.

The element ATF-MQ is used for this computation by using two meshes given by Fig. 6.14 in which the numbers of the elements are 12 and 48, respectively. The thickness-radius ratios h/R of the circular plate vary from 10^{-30} to 0.35. And, the relative precisions for the central deflection and bending moment are listed in Table 14.5.

From Table 14.5, it can be seen again that, the element ATF-MQ is universal for both thick and thin plates, and no shear locking happens. It provides high precision for both deflection and bending moment. When 48 elements are used, all errors are around or below 1%.

Example 14.6 Sensitivity test for mesh distortion.

The central deflections of the simply-supported and clamped square plates under uniformly distributed load are computed by using two distorted meshes shown in Fig. 14.6. Three distortion parameter cases: $\dfrac{\Delta}{0.5L} = 0.05$, 0.10 and 0.12 (or 0.20), are considered. The relative precision is given in Table 14.6.

From Table 14.6, it can be seen that, the element ATF-MQ is insensitive to mesh distortion. For various values of the distortion parameter $\dfrac{\Delta}{L}$, high accuracy can all be obtained.

Table 14.5 The relative precisions for central deflection w_C and bending moment M_C of circular plate (ATF-MQ)

h/R	Central deflection w_C				Central bending moment M_C			
	Simply-supported		Clamped		Simply-supported		Clamped	
	12 elements	48 elements	12 elements	48 elements	12 elements	48 elements	12 elements	48 elements
10^{-30}	1.0103	1.0024	0.9625	0.9898	1.0208	1.0040	1.0137	1.0002
0.001	1.0103	1.0024	0.9625	0.9898	1.0208	1.0040	1.0137	1.0002
0.01	1.0103	1.0024	0.9625	0.9898	1.0207	1.0041	1.0136	1.0003
0.10	1.0100	1.0025	0.9631	0.9905	1.0199	1.0046	1.0107	1.0014
0.15	1.0099	1.0025	0.9648	0.9913	1.0194	1.0047	1.0086	1.0014
0.20	1.0099	1.0026	0.9673	0.9922	1.0190	1.0047	1.0068	1.0011
0.25	1.0098	1.0026	0.9703	0.9930	1.0188	1.0047	1.0053	1.0007
0.30	1.0097	1.0026	0.9732	0.9938	1.0187	1.0046	1.0041	1.0002
0.35	1.0096	1.0025	0.9762	0.9945	1.0186	1.0045	1.0031	0.9997

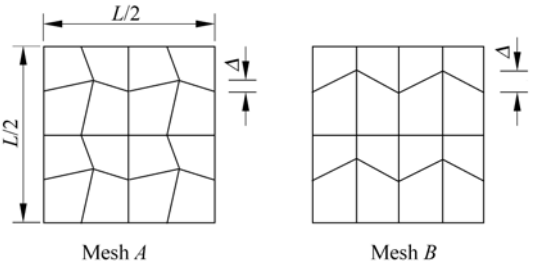

Figure 14.6 Two distorted meshes (for 1/4 square plate)

Table 14.6 The relative precision for central deflection of square plate by using distorted meshes (ATF-MQ)

Mesh	Distortion parameter $\frac{\Delta}{0.5L}$	Clamped		Simply-supported	
		Thickness-span ratio $h/L = 0.1$	Thickness-span ratio $h/L = 0.001$	Thickness-span ratio $h/L = 0.1$	Thickness-span ratio $h/L = 0.001$
Mesh *A*	0.05	1.0246	1.0152	1.0013	1.0093
	0.10	1.0500	1.0480	1.0074	1.0079
	0.12	1.0559	1.0573	1.0092	1.0071
Mesh *B*	0.05	1.0186	1.0091	1.0001	1.0096
	0.10	1.0348	1.0284	0.9958	1.0078
	0.20	1.0567	1.0481	1.0075	0.9942

14.6 Analytical Trial Function Method for Developing a Triangular Thick Plate Element Based on a Thin Plate Element

In this section, the analytical trial function (ATF) method is used to extend the existing Kirchhoff triangular thin plate element to the corresponding Mindlin triangular thick plate element. As an example, the triangular thin plate element GPL, proposed in reference [19], is generalized to a thick/thin plate element GPLM (M denotes the Mindlin plate).

14.6.1 Brief Review of the Triangular Thin Plate Element GPL

This element possesses only 9 DOFs. The element nodal displacement vector is

$$\boldsymbol{q}^e = [w_1 \quad \psi_{x1} \quad \psi_{y1} \quad w_2 \quad \psi_{x2} \quad \psi_{y2} \quad w_3 \quad \psi_{x3} \quad \psi_{y3}]^{\mathrm{T}} \tag{14-22}$$

According to the ATF method, the element deflection and rotation fields are assumed to be

$$\left.\begin{aligned} w &= \boldsymbol{F}\boldsymbol{\lambda} \\ \psi_x &= \frac{\partial w}{\partial x} = \frac{\partial}{\partial x}\boldsymbol{F}\boldsymbol{\lambda} \\ \psi_y &= \frac{\partial w}{\partial y} = \frac{\partial}{\partial y}\boldsymbol{F}\boldsymbol{\lambda} \end{aligned}\right\} \tag{14-23}$$

in which $\boldsymbol{\lambda}$ contains 9 unknown coefficients; and $\boldsymbol{F}$ is composed of 9 trial functions

$$\begin{aligned} \boldsymbol{F} = \Bigg[& L_1 \quad L_2 \quad L_3 \quad L_1L_2 \quad L_2L_3 \quad L_3L_1 \quad L_1\left(L_1 - \frac{1}{2}\right)(L_1 - 1) \\ & L_2\left(L_2 - \frac{1}{2}\right)(L_2 - 1) \quad L_3\left(L_3 - \frac{1}{2}\right)(L_3 - 1) \Bigg] \end{aligned} \tag{14-24}$$

Since the highest order of these trial functions F is cubic, thereby, they satisfy the bi-harmonic Eq. (14-12). For the thin plate theory, these trial functions are all the analytical trial functions.

For solving the 9 unknown coefficients, 9 conforming conditions are selected as follows

$$(w - \overline{w})_i = 0 \qquad \text{(for each corner node } i = 1,2,3) \tag{14-25a}$$

$$\int_{d_j} (w - \overline{w})\mathrm{d}s = 0 \qquad \text{(for each side } d_j = d_1, d_2, d_3) \tag{14-25b}$$

$$\int_{d_j} (\psi_n - \overline{\psi}_n)\mathrm{d}s = 0 \qquad \text{(for each side } d_j = d_1, d_2, d_3) \tag{14-25c}$$

Then, $\boldsymbol{\lambda}$ can be derived from the above equations, and can be expressed in terms of $\boldsymbol{q}^e$

$$\boldsymbol{\lambda} = \boldsymbol{P}\boldsymbol{q}^e \tag{14-26}$$

Substituting the above equation back into Eq. (14-23), the element displacement fields and its shape functions can be determined. And then, the element stiffness matrix $\boldsymbol{K}^e$ can be derived following the conventional procedure.

14.6.2 Generalization of the Element GPL to the Triangular Thick Plate Element GPLM

In the thick plate element, $\boldsymbol{q}^e$ is still given by Eq. (14-22).

Based on the analytical solutions (14-13) of the thick plate theory, the displacement fields (14-23) of the element GPL are generalized to the following forms

$$\left.\begin{aligned} w &= \left(\boldsymbol{F} - \frac{D}{C}\nabla^2\boldsymbol{F}\right)\boldsymbol{\lambda} \\ \psi_x &= \frac{\partial}{\partial x}\boldsymbol{F}\boldsymbol{\lambda} \\ \psi_y &= \frac{\partial}{\partial y}\boldsymbol{F}\boldsymbol{\lambda} \end{aligned}\right\} \tag{14-27}$$

The expressions in the above equation are the displacement fields of the thick plate element assumed according to the ATF method. Thus, from the above equation, the shear strains of the thick plate element can be obtained as follows

$$\left.\begin{aligned} \gamma_x &= \frac{\partial w}{\partial x} - \psi_x = -\frac{D}{C}\frac{\partial}{\partial x}\nabla^2\boldsymbol{F}\boldsymbol{\lambda} \\ \gamma_y &= \frac{\partial w}{\partial y} - \psi_y = -\frac{D}{C}\frac{\partial}{\partial y}\nabla^2\boldsymbol{F}\boldsymbol{\lambda} \end{aligned}\right\} \tag{14-28}$$

It can be seen that, when the plate becomes thinner, Eq. (14-27) will degenerate to be Eq. (14-23) of the thin plate element, and Eq. (14-28) will degenerate to be

$$\gamma_x = 0, \quad \gamma_y = 0 \tag{14-29}$$

In order to solve the unknown coefficients in $\boldsymbol{\lambda}$, the conforming conditions (14-25a,b,c) for the thin plate element are still used, in which the original

displacement $\bar{w}$ along the element boundary should be replaced by the boundary displacement $\bar{w}^*$ of the thick plate element

$$\left.\begin{aligned} &(w-\bar{w}^*)_i = 0 \quad \text{(for each corner node } i=1,2,3) \\ &\int_{d_j}(w-\bar{w}^*)\mathrm{d}s = 0 \quad \text{(for each side } d_j = d_1, d_2, d_3) \\ &\int_{d_j}(\psi_n - \bar{\psi}_n)\mathrm{d}s = 0 \quad \text{(for each side } d_j = d_1, d_2, d_3) \end{aligned}\right\} \tag{14-30}$$

Then, we can obtain

$$\boldsymbol{\lambda} = \boldsymbol{P}^* \boldsymbol{q}^e \tag{14-31}$$

When the plate becomes thinner, Eqs. (14-30) and (14-31) will degenerate to be Eqs. (14-25) and (14-26) which are used for the thin plate element.

The main procedure for the generalization of the element GPL to the element GPLM has been described above. This generalization can be performed conveniently.

By the comparison of the new and old elements, it can be seen that their derivation procedures are the same, and formulae in each step are also similar. The key step in this procedure is the assumption of displacement fields according to the analytical trial function method, in which Eq. (14-23) of the original element is replaced by Eq. (14-27) of the new element. In these two equations, except that there is a $-\dfrac{D}{C}\nabla^2 \boldsymbol{F}\boldsymbol{\lambda}$ term in the deflection expression of Eq. (14-27), the other expressions are exactly the same. Only one term is different, so the new and old elements are quite similar in form.

However, although only one term is different, the effects of this term $\left(-\dfrac{D}{C}\nabla^2 \boldsymbol{F}\boldsymbol{\lambda}\right)$ is very pivotal—By this term, the shear strains can be introduced into the new thick plate element; and also by this term, the shear locking phenomenon of the new thick plate element can be successfully eliminated.

Though the method proposed in this section is described by taking the element GPL as an example, in fact, it can also be used to generalize other existing triangular and quadrilateral thin plate elements to the corresponding thick/thin elements, as long as the trial functions for the deflections of these existing thin plate elements are the analytical trial functions of thin plate theory, i.e., should be the bi-harmonic functions.

There are several successful schemes that can generalize the thin plate element to thick/thin one. What is introduced here is only one of them, and can be called as the analytical trial function (ATF) method. Another scheme is the rational interpolation technique in which the shear strain fields are directly introduced

into a thin plate (refer to Sects. 8.5 and 8.6). The triangular thick/thin element TCGC given in Sect. 8.6 is just derived by the latter scheme. When the plate becomes thinner, the element TCGC will also degenerate to be the element GPL. (It can be seen that the elements GPLM and TCGC are the two thick/thin plate elements generalized from the element GPL by the above two approaches.)

14.6.3 Numerical Examples

Example 14.7 Simply-supported and clamped square plates subjected to uniform load q.

As shown in Fig. 14.7, due to the symmetry, only a quarter of the plate is considered. The results obtained by four 8×8 meshes are listed in Table 14.7. The side length of the square plate is L, The Poisson's ratio $\mu = 0.3$.

From Table 14.7, it can be seen that

(1) when the plate becomes thinner, the thin plate element GPL-T9 is the final limit, thus, no shear locking will happen;

(2) the rational results can all be provided when the thickness-span ratio h/L varies from 10^{-30} to 0.35;

(3) the present element is insensitive to mesh distortion. For the four meshes Ⅰ, Ⅱ, Ⅲ and IV, errors given in Table 14.7 are all very small.

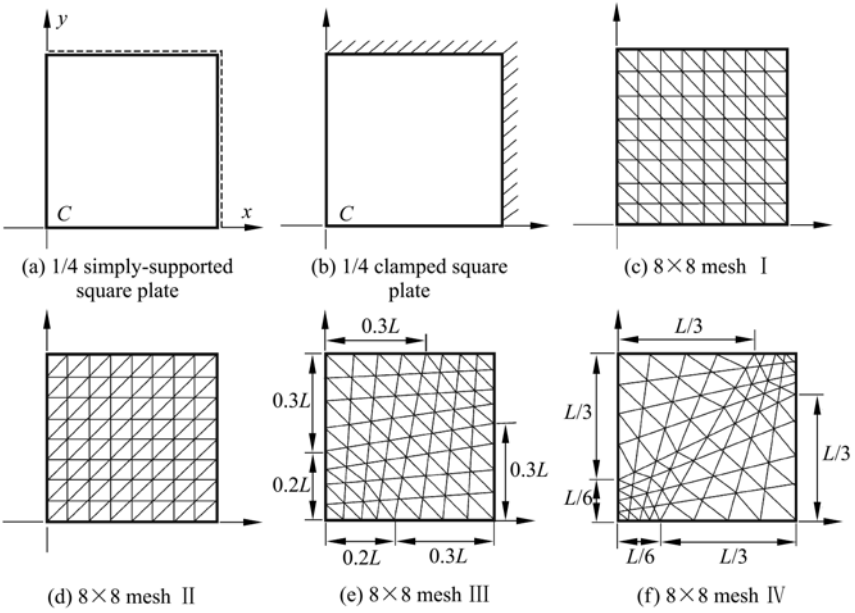

Figure 14.7 Simply-supported and clamped square plates

Table 14.7 The central deflection $w_C \Big/ \left(\frac{qL^4}{100D}\right)$ of square plate under uniform load (four 8×8 meshes Ⅰ, Ⅱ, Ⅲ and Ⅳ are used)

	Simply-supported square plate					Clamped square plate				
h/*L*	Mesh Ⅰ	Mesh Ⅱ	Mesh Ⅲ	Mesh Ⅳ	Analytical solution	Mesh Ⅰ	Mesh Ⅱ	Mesh Ⅲ	Mesh Ⅳ	Analytical solution
10^{-30}	0.4057 (99.88%)	0.4050 (99.70%)	0.4059 (99.93%)	0.4058 (99.90%)	0.4062	0.1247 (98.58%)	0.1261 (99.68%)	0.1252 (98.97%)	0.1254 (99.13%)	0.1265
0.01	0.4058 (99.85%)	0.4051 (99.68%)	0.4060 (99.90%)	0.4060 (99.90%)	0.4064	0.1249 (98.74%)	0.1263 (99.84%)	0.1255 (99.21%)	0.1256 (99.29%)	0.1265
0.10	0.4260 (99.70%)	0.4255 (99.58%)	0.4261 (99.72%)	0.4261 (99.72%)	0.4273	0.1480 (98.73%)	0.1502 (100.20%)	0.1494 (99.67%)	0.1492 (99.53%)	0.1499
0.15	0.4519 (99.63%)	0.4520 (99.65%)	0.4522 (99.69%)	0.4523 (99.71%)	0.4536	0.1759 (97.83%)	0.1788 (99.44%)	0.1780 (99.00%)	0.1773 (98.61%)	0.1798
0.20	0.4882 (99.51%)	0.4891 (99.69%)	0.4887 (99.61%)	0.4889 (99.65%)	0.4906	0.2138 (98.66%)	0.2175 (100.37%)	0.2168 (100.05%)	0.2156 (99.49%)	0.2167
0.25	0.5350 (99.46%)	0.5368 (99.80%)	0.5357 (99.59%)	0.5360 (99.65%)	0.5379	0.2616 (97.79%)	0.2665 (99.63%)	0.2658 (99.36%)	0.2639 (98.65%)	0.2675
0.30	0.5921 (99.41%)	0.5951 (99.92%)	0.5931 (99.58%)	0.5936 (99.66%)	0.5956	0.3195 (99.01%)	0.3257 (100.93%)	0.3251 (100.74%)	0.3224 (99.91%)	0.3227
0.35	0.6595 (99.31%)	0.6640 (99.98%)	0.6610 (99.53%)	0.6616 (99.62%)	0.6641	0.3876 (98.10%)	0.3953 (100.05%)	0.3949 (99.95%)	0.3911 (98.99%)	0.3951

Note: Numbers in ( ) are percentage precisions.

Example 14.8 Circular plate under uniform load.

Two boundary conditions are considered: soft simply-supported and clamped. As shown in Fig. 14.8, due to the symmetry, only a quarter of the circular plate is computed. The radius of the circular plate $R = 5$; and the Poisson's ratio $\mu = 0.3$.

Numerical results obtained by the present element GPLM are listed in Tables 14.8 and 14.9. For comparison, the results by the other elements T3BL, T3BL(R)[20], DKMT[21], DST-BK[22] and DST-BL[23] are also given.

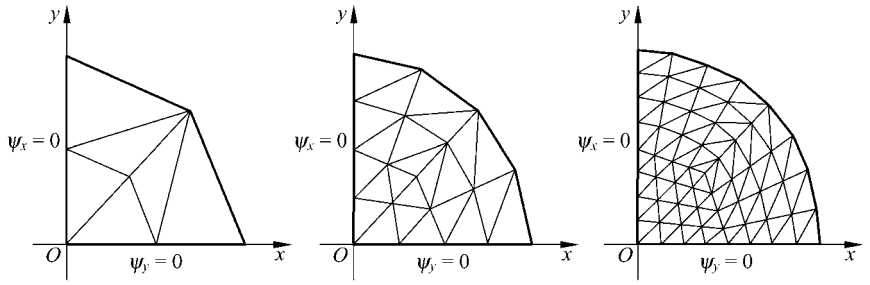

Figure 14.8 Meshes for circular plate

From Table 14.8, it can be seen that, in comparison with the similar elements, the element GPLM can give the best results for the central bending moment of clamped square plate. And, from Table 14.9, it can also be seen that the element GPLM can produce the best answers for the central deflection and bending moment of the simply-supported plate.

Table 14.8 The central deflection $w_C \Big/ \left(\frac{qR^4}{D} \right)$ and bending moment M_C / qR^2 of clamped circular plate

	$h/R = 0.002$						$h/R = 0.2$					
	GPLM	T3BL	T3BL (R)	DKMT	DST-BK	DST-BL	GPLM	T3BL	T3BL (R)	DKMT	DST-BK	DST-BL
Central deflection												
6 elements	7.2283	6.0495	9.1192	10.3060	9.8430	10.3060	8.7991	8.0392	10.8377	11.921	11.342	11.951
24 elements	9.0867	8.7750	9.6403	9.9956	9.8551	9.9958	10.7473	10.6006	11.4059	11.703	11.548	11.806
96 elements	9.6038	9.5237	9.7382	9.8748	9.8025	9.8483	11.3344	11.3022	11.5066	11.594	11.554	11.731
Analytical	9.7835						11.5513					
Central bending moment												
6 elements	2.0315	1.2188	1.3304	2.40	2.56	2.40	2.0010	1.2885	1.3296	2.47	2.31	2.43
24 elements	2.0535	1.8187	1.8354	2.17	2.25	2.17	2.0498	1.8258	1.8316	2.22	2.16	2.19
96 elements	2.0383	1.9771	1.9789	2.07	2.09	2.07	2.0317	1.9780	1.9784	2.09	2.07	2.10
Analytical	2.0313											

Table 14.9 The central deflection $w_C \Big/ \left(\frac{qR^4}{D} \right)$ and bending moment M_C / qR^2 of simply-supported circular plate

	$h/R = 0.002$						$h/R = 0.2$					
	GPLM	T3BL	T3BL (R)	DKMT	DST-BK	DST-BL	GPLM	T3BL	T3BL (R)	DKMT	DST-BK	DST-BL
Central deflection												
6 elements	40.2358	39.4319	42.2158	37.848	37.391	37.847	41.8163	41.1627	43.9038	39.462	38.888	39.494
24 elements	39.9018	39.6576	40.4609	39.398	39.249	39.397	41.5706	41.4296	42.2235	41.091	40.926	41.185
96 elements	39.8455	39.7848	39.9434	39.729	39.680	39.729	41.5771	41.5555	41.7594	41.473	41.432	41.705
Analytical	39.8315						41.5994					
Central bending moment												
6 elements	5.4548	4.7084	4.7486	5.26	5.43	5.26	5.4238	4.7237	4.7460	5.33	5.27	5.30
24 elements	5.2563	5.0310	5.0380	5.23	5.28	5.23	5.2345	5.0294	5.0342	5.27	5.22	5.25
96 elements	5.1835	5.1242	5.1217	5.18	5.20	5.18	5.1768	5.1239	5.1243	5.20	5.18	5.22
Analytical	5.1563											

References

[1] Long YQ, Zhi BC, Kuang WQ, Shan J (1982). Sub-region mixed finite element method for the calculation of stress intensity factor. In: He GQ et al. (eds). Proceedings of International Conference on FEM. Science Press, Shanghai, pp738 – 740

[2] Zhong WX, Ji Z (1996). Rational finite element. Computational Structural Mechanics and Applications 1: 1 – 8 (in Chinese)

[3] Long YQ, Fu XR (2002) Two generalized conforming quadrilateral thick plate elements based on analytical trial functions. Gong Cheng Li Xue/Engineering Mechanics 19(3): 10 – 15 (in Chinese)

[4] Fu XR, Long YQ (2002) Generalized conforming quadrilateral plane elements based on analytical trial functions. Gong Cheng Li Xue/Engineering Mechanics 19(4): 12 – 16 (in Chinese)

[5] MacNeal RH (1989) Toward a defect-free four-noded membrane element. Finite Elements in Analysis and Design 5: 31 – 37

[6] Long YQ, Fu XR (2002) Generalized conforming elements based on analytical trial functions. In: Proceedings of the Eleventh National Conference on Structural Engineering (Vol. Ⅰ), plenary lecture. China, Changsha, pp28 – 39 (in Chinese)

[7] Taylor RL, Beresford PJ, Wilson EL (1976) A non-conforming element for stress analysis. International Journal for Numerical Methods in Engineering 10: 1211 – 1219.

[8] Pian THH, Sumihara K (1984) Rational approach for assumed stress finite element. International Journal for Numerical Methods in Engineering 20: 1685 – 1695

[9] Andelfinger U, Ramm E (1993) EAS-elements for two dimensional, three dimensional, plate and shell structures and their equivalence to HR-elements. International Journal for Numerical Methods in Engineering 36: 1311 – 1337

[10] Cao YP, Hu N, Yao ZH (2002) Improved EAS elements. Gong Cheng Li Xue/Engineering Mechanics 19(1): 47 – 51 (in Chinese)

[11] Hu HC (1984) Variational principles of theory of elasticity with applications. Science Press, Beijing

[12] Zienkiewicz OC, Taylor RL, Too JM (1971) Reduced integration techniques in general of plates and shells. International Journal for Numerical Methods in Engineering 3: 275 – 290

[13] Hughes TJ, Cohen M, Haroun M (1978) Reduced and selective integration techniques in finite element analysis of plates. Nuclear Engineering and Design 46: 203 – 222

[14] Soh AK, Long ZF, Cen S (1999) A Mindlin plate triangular element with improved interpolation based on Timoshenko's beam theory. Communications in Numerical Methods in Engineering 15(7): 527 – 532

[15] Soh AK, Long ZF, Cen S (1999) A new nine dof triangular element for analysis of thick and thin plates. Computational Mechanics 24(5): 408 – 417

[16] Soh AK, Cen S, Long YQ, Long ZF (2001) A new twelve DOF quadrilateral element for analysis of thick and thin plates. European Journal of Mechanics A/Solids 20(2): 299 – 326

[17] Cen S, Long YQ, Yao ZH, Chiew SP (2006) Application of the quadrilateral area coordinate method: a new element for Mindlin-Reissner plate. International Journal for Numerical Methods in Engineering 66(1): 1 – 45

[18] Long ZF, Cen S (2001) New monograph of finite element method: principle, programming, developments. China Hydraulic and Water-power Press, Beijing (in Chinese)

[19] Long YQ, Bu XM, Long ZF, Xu Y (1995) Generalized conforming plate bending elements using point and line compatibility conditions. Computers & Structures 55(4): 717 – 728

[20] Taylor RL, Auricchio F (1993) Linked interpolation for Reissner-Mindlin plate element: part Ⅱ—a simple triangle. International Journal for Numerical Methods in Engineering 36: 3057 – 3066

[21] Katili I (1993) A new discrete Kirchhoff-Mindlin element based on Mindlin-Reissner plate theory and assumed shear strain fields—Part Ⅰ: An extended DKT element for thick-plate bending analysis. International Journal for Numerical Methods in Engineering 36: 1859 – 1883

[22] Batoz JL, Katili I (1992) On a simple triangular Reissner/Mindlin plate element based on incompatible modes and discrete constraints. International Journal for Numerical Methods in Engineering 35: 1603 – 1632

[23] Batoz JL, Lardeur P (1989) A discrete shear triangular nine d.o.f. element for the analysis of thick to very thin plates. International Journal for Numerical Methods in Engineering 28: 533 – 560